Proceedings of GT2011
ASME Turbo Expo
June 6-11, 2011, Vancouver, British Columbia, Canada

GT2011-45228

CASE STUDY OF MORTON EFFECT SHAFT DIFFERENTIAL HEATING IN A VARIABLE-SPEED ROTATING ELECTRIC MACHINE

Joshua A. Lorenz
Kato Engineering
Mankato, Minnesota, USA

Brian T. Murphy
Center for Electromechanics
University of Texas
Austin, Texas, USA

ABSTRACT

Hydrodynamic journal bearings can exhibit a particular form of Shaft Differential Heating (SDH) sometimes known as the Morton Effect. This paper presents test data of the Morton Effect in the form of synchronous spiral vibration observed in a 4200 rpm rotating electric machine. With its original partial arc bearings, divergent spiral vibration prevented stable operation above 4000 rpm. Subsequent analytical SDH studies of different bearing types are described which led to a switch to 4 lobe sleeve bearings. The 4 lobe bearing retrofit eliminated the unstable spiral vibration behavior. To the authors' knowledge, this is the first published instance of a verified case of the Morton Effect to be solved exclusively by a change in bearing hardware with no accompanying changes to the rotor, shaft or journal.

INTRODUCTION

Shaft Differential Heating (SDH) in fluid-film bearings and its corresponding circumferential temperature gradients have been present, whether it be transient or steady-state, since the inception and industrial usage of fluid-film bearings around the turn of the 19th century. There has long been a commonly adopted assumption that any circumferential temperature gradients in the shaft of a fluid-film bearing are only transient in time with a period of one shaft revolution, and limited to a relatively small radial depth of penetration (i.e. skin depth) in the shaft. The time-averaged steady-state temperature of every point around the circumference of the shaft is generally assumed to be equivalent, and the shaft surface temperature is subsequently treated as circumferentially isothermal. Assumptions of this type are commonplace in industrial bearing design codes used today.

The development of steady-state circumferential shaft temperature gradients in the fluid-film bearing region of a rotating shaft leads to a thermally induced bend in the shaft. Non-uniform thermal expansion of the shaft material causes one side of the shaft to elongate relative to the other, which in turn produces a bend in the shaft. Under certain circumstances, the bend in the shaft can be significant enough to produce an unstable synchronous rotordynamic response due to the increased imbalance forces. This potentially troublesome machinery vibration phenomenon is generally referred to as the Morton Effect [1]. A thorough review of literature on this topic is given by DeJongh [2].

Kato Engineering has recently been involved with a particular variable-speed rotating electric machine design which exhibited problematic symptoms of the Morton Effect. Divergent spiral vibrations (as observed on a polar plot of synchronous vibration response) are a symptom of the Morton Effect which was exhibited by the machine. Most rotating machines are not measurably affected by shaft circumferential temperature gradients, and do not succumb to the negative consequences of the Morton Effect. Some machine configurations, however, are sensitive to the Morton Effect. A common trait is a significant mass overhung outboard of one or both bearings. Shaft bending at the bearing throws the overhung mass out of balance. If the machine is running at a speed where vibration amplitude at the bearing is sensitive to imbalance of the overhung mass, then conditions that produce a Morton Effect instability may be satisfied. The machine referenced in this case study had a significant overhung mass outboard of one of the bearings.

This paper presents detailed vibration data and discusses the bearing analysis that led to the resolution of the instability.

No design specifics of the machine itself are presented, however, due to its proprietary nature.

NOMENCLATURE

A	Balance sensitivity vector (microns/kg-mm)
B	Temperature coefficient vector (°C/micron)
C	Bow coefficient vector (kg-mm/°C)
L	Bearing axial length (micron)
L_w	Axial distance from bearing to overhung mass (mm)
M	Amount of overhung mass (kg)
R	Shaft radius at the bearing (mm)
s	Complex eigenvalue (1/seconds)
T	Shaft temperature difference vector (°C)
U	Imbalance vector, or heavy spot (kg-mm)
V	Vibration vector, or high spot (microns)
α	Coefficient of thermal expansion (1/°C)
τ	Time constant (seconds)

THE MORTON EFFECT ANALYSIS METHOD

A method for simplified analysis of rotordynamic instability due to the Morton Effect has been proposed by Murphy and Lorenz [3]. The complete method of analysis can be broken down into 13 steps. Descriptions of the steps in the analysis process are provided here. More information on each step in the process can also be found in [3].

The Morton Effect stability analysis method can be used for any type of journal bearing for which a typical steady state bearing design analysis code is available. A requirement of the bearing code utilized is that the steady state circumferential temperature profile of the lubricant be available for post processing. The ability to perform a rotordynamic imbalance response analysis is a further requirement of the process. Rotordynamic instability due to the Morton Effect is assessed as follows:

1. For a selected combination of machine rpm speed and bearing load, run the bearing analysis program to compute the journal static eccentricity position, and the linearized stiffness and damping coefficients of the bearing.

2. Run a rotordynamic imbalance response analysis of the subject machine to calculate a journal orbit at the bearing of interest. Figure 1 shows an example journal orbit calculated from a rotordynamic imbalance response analysis along with static eccentricity calculated from the bearing analysis program. For the case study results shown here, the initial imbalance for all response analyses was applied at the CG of the overhung weight and a magnitude of 25.2 kg-mm was utilized. An imbalance magnitude which results in orbit sizes which are reasonably commensurate with expected vibration levels (in the absence of an instability) are recommended.

   The selected imbalance weight of 25.2 kg-mm is similar to the magnitude of trial weights found to be effective for in situ balancing on the overhung mass during factory testing. As discussed in reference [3], the results of the Morton effect analysis are not sensitive to this amount.

3. Run the bearing analysis program again, but specify the position of the journal center to be the point corresponding to the ‘high spot’ in Fig. 2. This is the instant when the film thickness is at its minimum value due to the journal orbital position being closest to the bearing wall. The bearing program produces a circumferential oil film temperature profile around the bearing. At this point in time, the instantaneous shaft surface circumferential temperature profile (under the bearing) is assumed to be equal to the calculated oil film circumferential temperature profile. For this case study, the oil film temperatures utilized from the bearing program are the mean film temperatures.

4. Repeat the calculations done in the preceding step with the journal positioned at successive locations around the orbit path. Reference [3] recommends using 24 equally spaced points along the orbit. Since the clocking of the journal is also progressing as the journal travels around the orbit, an instantaneous shaft surface circumferential temperature profile is established in the rotating reference frame of the shaft.

5. Upon completion of the preceding steps, multiple values of temperature are obtained for any location on the shaft surface. The number of temperature values obtained for each point on the shaft is equivalent to the number of discretized points in the orbit path (24 for these cases). The temperature values at a given location on the shaft are then averaged to yield the final calculated steady-state circumferential temperature profile on the shaft surface.

6. From the calculated steady-state shaft circumferential temperature profile of step 5, a shaft delta T value is computed (temperature difference between minimum and maximum values around the circumferential profile).

7. Assume a shaft hot spot lag angle of 30 degrees. Further discussion of hot spot phase angle and its computational complexities are found in [3] as well as recent work by Lorenz [4]. Actual values are believed to lie in the range of 0 to 60 degrees (lagging) and an approximate mean value of 30 degrees was used for this case study.

8. Using the data from steps 6 and 7 as well as the imbalance response orbit size from step 2, calculate the shaft temperature coefficient vector ($\vec{B}$). This is the sensitivity of the shaft temperature difference to vibration amplitude at the bearing.

9. Use the rotordynamic imbalance response model from step 2 and calculate the influence coefficient vector for response at the bearing due to imbalance at the overhang ($\vec{A}$). This is the sensitivity of the vibration response at the bearing to imbalance at the overhung mass.

10. Calculate the shaft bow coefficient vector utilizing Eq. (1) (from [5]) to estimate the amount of imbalance produced at the overhang for a given shaft temperature differential at the bearing ($\vec{C}$). This is the sensitivity of imbalance at the overhang to shaft temperature difference at the bearing.

11. Calculate the dimensionless complex product $\vec{B}\vec{A}\vec{C}$. The real part of this is the stability parameter for the Morton Effect at a given speed [3].

12. Repeat steps 1 through 11 for each speed of interest.

13. Collect the stability parameter results at each speed analyzed and plot the stability parameter results in the complex plane. Use the stability criterion described in [3] (shown here as Eq. (2)) to evaluate the machine susceptibility to the Morton Effect at a given speed. Stability parameter results which have positive real parts exceeding 1.0 are considered unstable (i.e. the machine would be expected to exhibit divergent spiral vibration). The threshold for stability is not arbitrary but in fact based on closed-loop control system theory. Further details of the closed-loop control system analogy for Morton Effect are provided in [4].

$$U_{th} = M\frac{\alpha T}{R}LL_w \tag{1}$$

$$\mathrm{Re}\left(\vec{B}\vec{A}\vec{C}\right) \leq 1 \quad \text{for stability} \tag{2}$$

The accuracy of the Morton Effect stability analysis method was found to be dependent on the oil film temperature profiles computed in the bearing program. Many industrial fluid film bearing analysis codes have numerous options for the thermal modeling aspects. Therefore it is important to utilize options in the bearing analysis which produce bearing temperature profiles in good agreement with available test data. In this particular case study this was found to be an important part of getting good agreement between the Morton Effect calculation and observed vibration behavior.

The analysis method also requires a fair amount of diligence to implement correctly. Potential problem areas lie in the usage of phase angle sign conventions, bearing oil film temperature profiles in shaft reference coordinates, assumed lubricant temperature profiles at the oil inlets, etc. For the calculations presented here, the complete calculation process which blends rotordynamic modeling, iterative bearing thermohydrodynamic simulations, and simple structural mechanics was performed by a Microsoft Excel Visual Basic routine.

CASE HISTORY

The first prototype machine was designed, built, and tested with partial arc bearings (Fig. 3). One end of the machine also contained an integral thrust bearing (TE). On the non-thrust end (NTE) there is a significant overhung mass. The pair of original bearings were essentially identical. They were fixed-arc bearings with a single oil-inlet port just above the horizontal split-line. The machine was designed as a variable speed unit with a maximum continuous operating speed of 4200 rpm. Multiple units were built and tested. The discovery of the divergent spiral vibration problem occurred during factory testing of the second unit built. An additional two units were built during the stage of problem diagnosis, bringing the total number of machines built with the original bearing configurations to four.

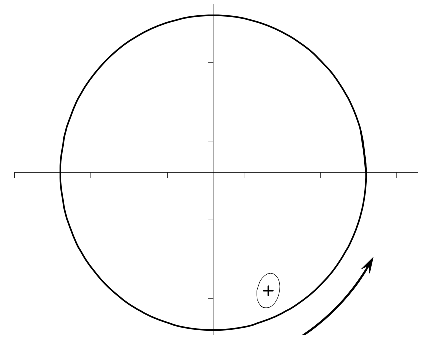

Figure 1. Bearing clearance circle and 1X orbit calculated at 3975 rpm with 25.2 kg-mm imbalance. Orbit is centered at static eccentricity position calculated with bearing code.

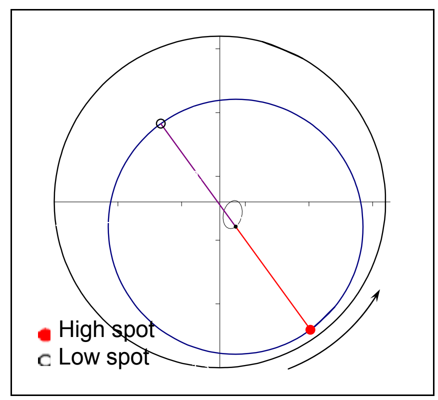

Figure 2. Journal and bearing with exaggerated clearance. Journal center and orbit calculated at 3975 rpm with 25.2 kg-mm imbalance. Journal instantaneous position is at moment of minimum film thickness.

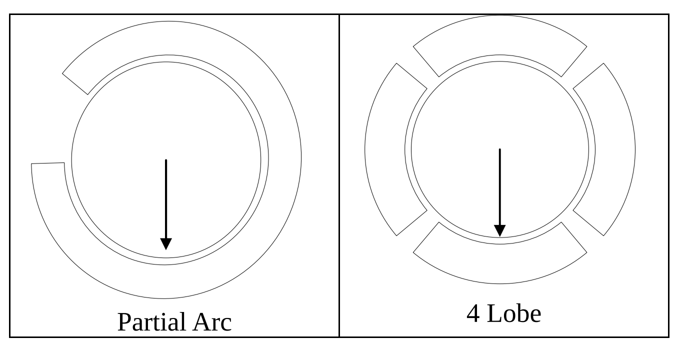

Figure 3. Schematics of tested bearing configurations.

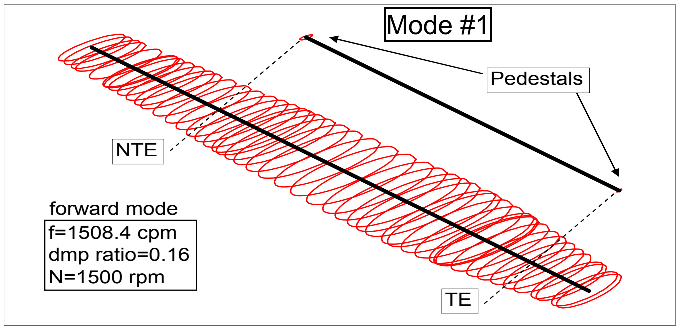

Figure 4. Calculated Rotordynamic Natural Mode 1.

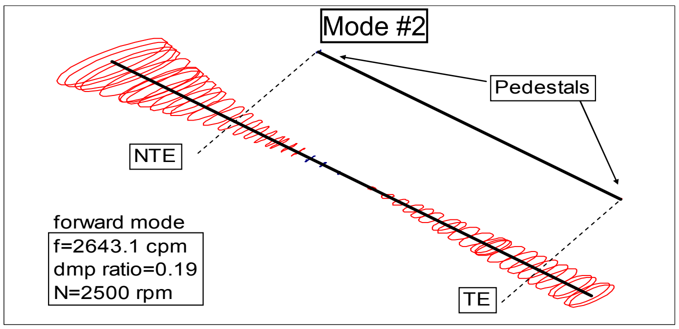

Figure 5. Calculated Rotordynamic Natural Mode 2.

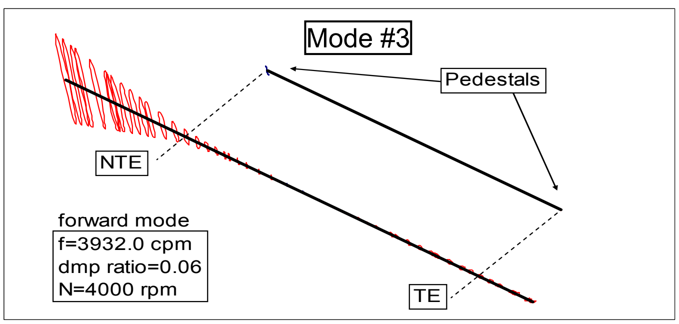

Figure 6. Calculated Rotordynamic Natural Mode 3.

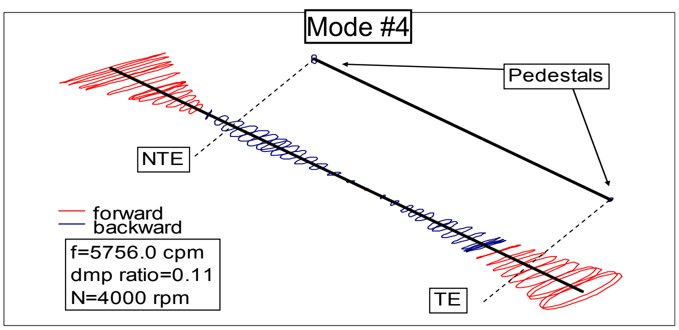

Figure 7. Calculated Rotordynamic Natural Mode 4.

Rotordynamic Response Analyses

Various rotordynamic analyses were performed prior to fabrication. Imbalance response analyses showed the machine to be super-critical in that multiple rotor flexible mode shapes were to be traversed during normal operation. One of the primary conclusions of the analytical work was: if the imbalance magnitudes of the rotor assembly were reasonably well controlled during manufacturing, the expected vibration response levels at the bearings during normal operation should be within the specification requirements.

The analysis revealed expected rotordynamic critical speeds near 1500, 2500, and 4000 rpm. Calculated mode shapes and corresponding frequencies for the rotordynamic natural frequencies occurring near these speeds are provided in Figures 4, 5 and 6. The next calculated mode was near 5700 cpm (Fig. 7). All analysis and figures were generated by a commercially available rotordynamic analysis software package [6]. The mode shape near 4000 rpm can be aptly described as flexing of the NTE shaft extension due to the NTE overhung mass. The 4th mode is well above maximum speed, but still can be important to the Morton Effect because it is dominated by motion of the overhung mass, and deflections at the overhung mass and at the nearby NTE bearing are out of phase.

Initial Factory Tests

One of the factory acceptance tests involved an extended run at 4200 rpm. It was during this extended constant speed test for unit 2 that the divergent spiral vibration behavior was first observed in a problematic and potentially damaging manner. Due to issues with the speed controller, the actual test speed set-point used for unit 2 was 4150 RPM . Vibration was monitored using eight vibration transducers. Four proximity probes were utilized (two at each bearing; 90 degrees apart), and four velocity probes (two near each bearing housing; mounted vertically and horizontally). Time-history traces of the synchronous (1x) vibration for the proximity probes are shown in Fig. 8. Velocity measurements exhibited the same characteristics. Note the similarity between the response curves and that of a harmonic function exhibiting exponential growth. The behavior is analogous to an unstable closed-loop feedback control system, and further discussion of the closed-loop feedback control system analogy can be found in [4]. The

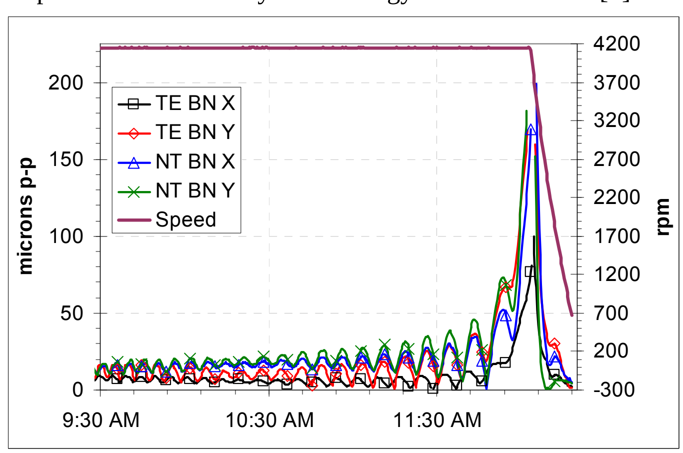

Figure 8. 4150 RPM Constant Speed Factory Test of Unit 2 – Prox Probes 1x Vibration Amplitude vs. Time.

factory acceptance test was eventually halted due to excessive vibration. Due to the slow thermal time scale associated with the changes in vibration magnitude, plus the fact a time-history plot was not monitored real-time during the test, and also that the somewhat rare symptoms of the Morton Effect were not known to the test operators at the time, the machine was not shut down until the vibration reached excessive and rapidly divergent levels. Polar plots of the synchronous vibration for the proximity probes are shown in Fig. 9. The divergent spirals (as viewed on the polar plots) were the primary piece of investigative information leading to the Morton Effect diagnosis. Polar plots are an effective way to recognize the presence of spiraling or circulatory vibration vectors (e.g. see reference [7]). Spiraling behavior in a polar plot can also be caused by the Newkirk Effect [2], which is another form of shaft differential heating similar to the Morton Effect, but is due to rubbing instead of shear in a bearing oil film. In our case, from other considerations we were able to eliminate rubbing as a potential cause.

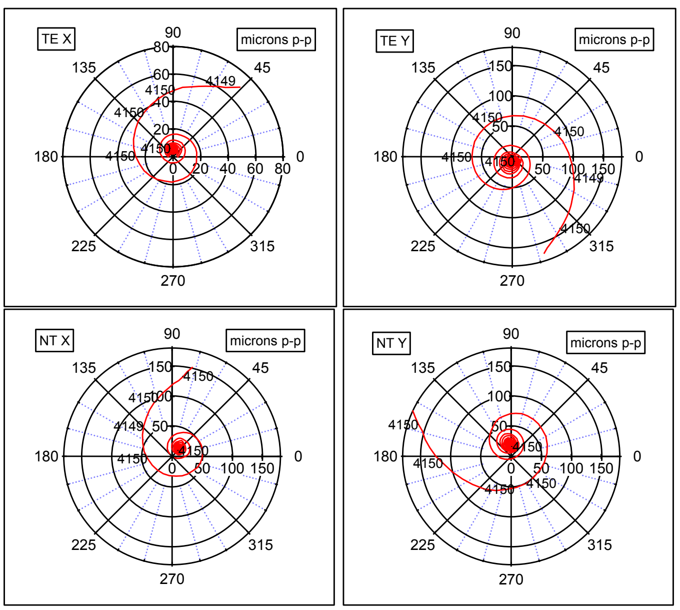

Figure 9. Polar plot of Fig. 8 data, excluding shutdown. Labels on curves are rpm.

Original Design Information & Test Data Compilation

Upon experiencing divergent vibration on unit 2, test data was re-examined for machines 1, 3, and 4, of which all were initially built with partial arc bearings. Data for multiple builds of the same basic machine revealed significant observations regarding the behavior of Morton Effect instability.

From the test data it was clear that the instability is an inconsistent phenomenon, suggesting sensitivity to one or more operational or assembly variables. The speed at which the instability starts to show itself, and the time it takes to evolve into a rapidly divergent vibration event were variable among the machines and also among different test runs for a given machine. Considering the complexities of the physics at play which lead to the Morton Effect, this is not surprising. Slight variations in bearing clearance, bearing alignment, ambient temperature, machine operating temperature, lubricant properties, overhung mass, support stiffness, etc. can all influence the physics of shaft differential heating and its potentially unstable rotordynamic response. A common trait of the machines was that they all showed signs of divergent spiral vibration on a thermal time scale near maximum continuous operating speed.

It is significant that after the instability was observed on unit 2 during factory testing at 4175 rpm, the machine was run at 4000 rpm and found to operate in a stable manner after the initial speed-change transient behavior settled out while running at 4000 rpm steady speed (i.e. converging spiral vibration). Based on this, it was decided to operate subsequent units at speeds not exceeding 4000 rpm, and this was hoped to be the final solution to the problem. Unit 1 was already in the field. Units 3 and 4 were yet to be built at that time. Unit 3 was eventually built, tested, and found to be oscillatory, yet not unstable, at 4000 rpm. Unit 4 was built and found to be unstable at 4000 rpm. The unstable behavior of unit 4 became the primary impetus for pursuit of a bearing configuration change. At the time of unit 4 testing, the behavior was reasonably well understood by the authors, but the Morton Effect was not universally accepted by all as the root cause of the vibration problem.

Coincidentally, it was near the time of the unit 4 event (i.e. unstable spiral at 4000 rpm) that the authors were able to bring together the new Morton Effect analysis method described in [3] and analyze the original bearing geometry, as well as potential bearing configuration changes to find a solution that could be implemented via a bearing liner hardware change. The unit 4 divergence presented a window of opportunity for using the analysis tools and proposing to the team a potential bearing change solution.

The specifics of the machine application are also noteworthy with regards to the relationship of the predicted rotor natural frequencies and the operating speed. The specifics of the application provide an understanding of potential reasons for the variability observed between machines during testing. The machine generally spends little time at a constant speed during factory testing. The primary exception is the extended run at maximum speed to verify thermal behavior. This extended run at maximum speed happens to be in the vicinity of a rotor flexible mode natural frequency, and more importantly a rotor flexible mode shape which is sensitive to imbalance at the NTE overhung mass. The machine is operated at a fairly well regulated speed during the test (whether it be 4200, 4150, 4000 rpm, etc.) while the natural frequency of the rotordynamic mode shape likely varies due to minor variations in the geometry as well as the manufacturing and testing processes (e.g. bearing clearance, bearing alignment, ambient temperature, machine operating temperature, lubricant properties, overhung mass, support stiffness, etc.). Note that some of these items can change during operation. The extended run maximum speed test for unit 1 was run at 4175 rpm due to issues with the variable frequency drive controller. The speed control of that particular test was notably more erratic than all subsequent tests. This is one possible reason the synchronous instability was not observed at 4175 rpm on unit 1 while performing the extended run. Another factor is that the constant speed test on unit 1 was carried out at a speed set-point which was 25 rpm further removed from the rotordynamic natural frequency near 4000 rpm. Small changes in the actual critical speed of the machine relative to the operating speed can have a significant impact on Morton Effect stability. Small changes in true rotordynamic critical speed manifest themselves as changes to the balance sensitivity vector ($\vec{A}$), which in-turn directly affects the computed stability parameter at a given speed. The first three units were all tested at different speed set-points for the extended run at maximum speed (4175, 4150, and 4000 rpm respectively). These subtle differences in test procedures may contribute to the observed variation in the Morton Effect instability from one machine to the next.

All rotordynamic calculations performed to-date have shown the presence of a rotor flexible mode shape near 4000 rpm, and the test data confirms those predictions. Identifying a precise value for the critical speed near 4000 rpm is clouded by Morton Effect symptoms, and the 'false critical speeds' that can occur on run-down of a machine exhibiting symptoms of the Morton Effect. This particular trait has been documented in a 2008 paper by Schmied, Pozivil, and Walch [7], among others. The phenomenon can also be thought of as a thermal bending hysteresis upon running the machine up and then back down in speed. As the machine operates at a constant speed in the unstable regime, the imbalance of the overhung mass continuously changes due to ever increasing shaft bending (i.e. divergent spiral behavior). When the machine is allowed to spin down, the resulting imbalance due to shaft bending generally does not subside until after the machine has already slowed, because of the thermal time scale of the Morton Effect phenomenon. This gives the illusion of a different critical speed in the spin-down plot (compared to spin-up) as shaft differential heating begins to dissipate. This phenomenon is demonstrated with test data for multiple machines in Figures 10-12 (arranged in chronological order). For the vibration test data shown in Fig. 11, unit 1 was run up and down between 3000, 3800, and 4200 rpm numerous times as part of its normal operation. During the rapid traverses from 3000 or 3800 rpm to 4200 rpm there is little time for the instability to develop while operating near maximum speed. Notice the presence of what appear to be varying critical speed peaks near 4100 rpm in the lower right-hand corner of Fig. 11. Eventually the machine was run for a more significant period of time at a constant speed of 4200 rpm. During this time the instability was able to develop, and rapid vibration amplitude growth was observed. The machine was shut-down due to high vibration, and upon final run-down there was a significant peak in the response at 3975 rpm due to imbalance of the overhung mass caused by shaft differential heating. The response peak at 3975 rpm is likely a good estimate of the true rotordynamic critical speed. In the figures, eventually the additional imbalance due to the Morton Effect dissipates, and the run-down vibration amplitude traces

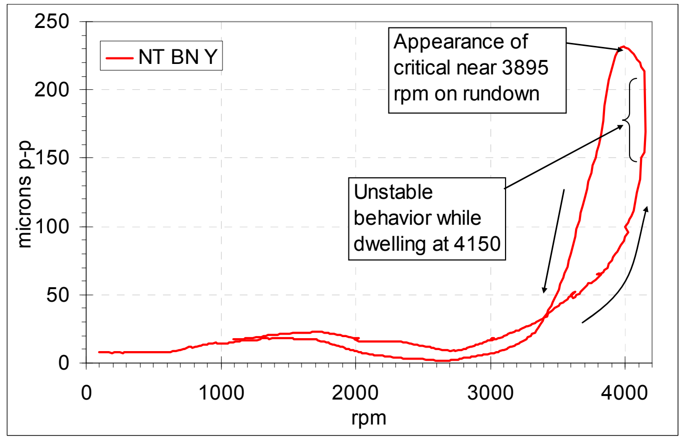

Figure 10. Unit 1 – Appearance of Critical Speed at 3985 RPM at Run-down from 4200 RPM.

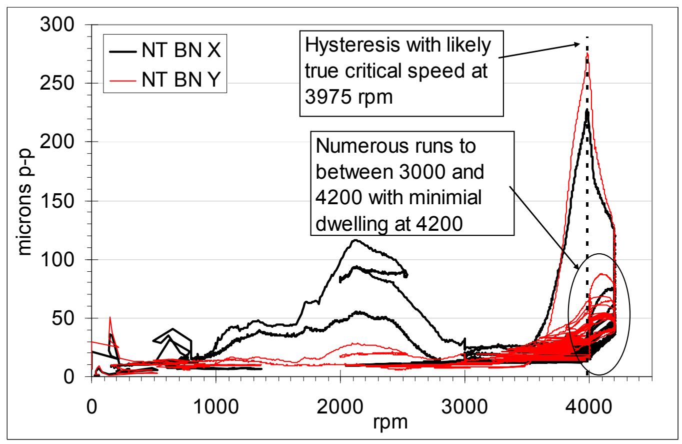

Figure 11. Unit 1 – Appearance of Critical Speed at 3975 RPM at Run-down from 4200 RPM – Off-Site Testing.

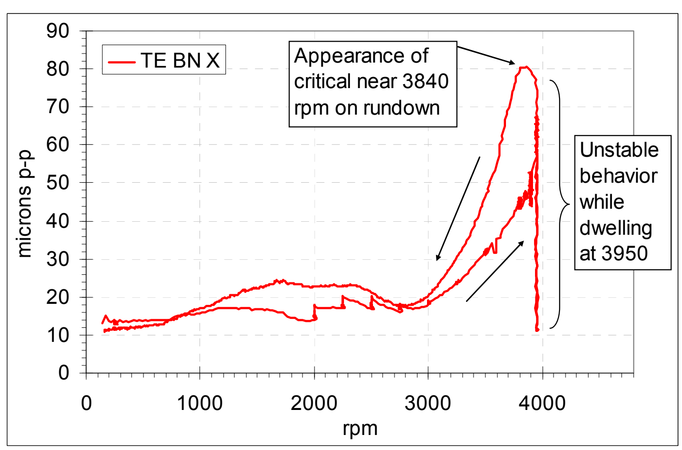

Figure 12. Unit 4 – Appearance of Critical Speed at 3840 RPM at Run-down from 3950 RPM.

Table 1. Summary of Oscillating and Divergent Events.

Event #	Unit #	Location	Speed (rpm)	Cyclic Period (sec)	Time Constant (sec)	Growth Rate %/Minute
1	1	Off-site	4200	436 sec	742	22%
2	1	Off-site	4200	467 sec	774	21%
3	1	Off-site	4200	456 sec	1045	16%
4	1	Off-site	4200	478 sec	1240	13%
5	1	Off-site	4200	800 sec	982	17%
6	2	Factory	4150	464 sec	2267	7%
7	2	Factory	4150	452 sec	792	21%
8	3	Factory	4100	462 sec	382	43%
9	4	Factory	4000	235 sec	92	177%
10	4	Factory	4000	272 sec	263	62%
11	4	Factory	4000	243 sec	731	22%
12	4	Factory	3950	477 sec	1052	16%

Table 2. Velocity Probe Nominal Synchronous Vibration Response Levels (mm/sec 0-pk).

Unit #	Near 2500 rpm critical speed	Upon Reaching 4000 rpm
1	2.0	2.0
2	1.3	2.0
3	0.8	0.5
4	0.4	0.6

start to track the run-up traces more closely, as would be expected for a stable operating machine.

The test data for the divergent events for all machines with original partial arc bearings was compiled and fitted with exponential harmonic functions to determine the time constant of exponential growth as well as the period of oscillation for each recorded event. The mathematics of the Morton Effect spiral response and its time constant are discussed in more detail in [3]. Twelve different divergent events involving units 1, 2, 3, and 4 were curve fit. On two separate occasions unit 3 oscillated without diverging while operating at 4000 rpm for more than two hours. The divergent behavior for unit 3 was experienced at 4100 rpm. The results of the curve-fitting operations for all twelve events are in summarized Table 1. Example vibration data along with the accompanying curve fit is shown in Fig. 13 for divergent event number 3. The data used for Fig. 13 is from unit 1 while being tested at its off-site location and prior to speed being capped at 4000 rpm. The period of oscillation from one event and one machine to the next is more consistent than the rate of divergence. For units 1, 2, and 3 the period of oscillation was generally about 7.5 minutes (450 seconds). Unit 4 had a measurably reduced period of oscillation of about 4 minutes. The time constant of exponential growth for units 1, 2, and 3 ranged from

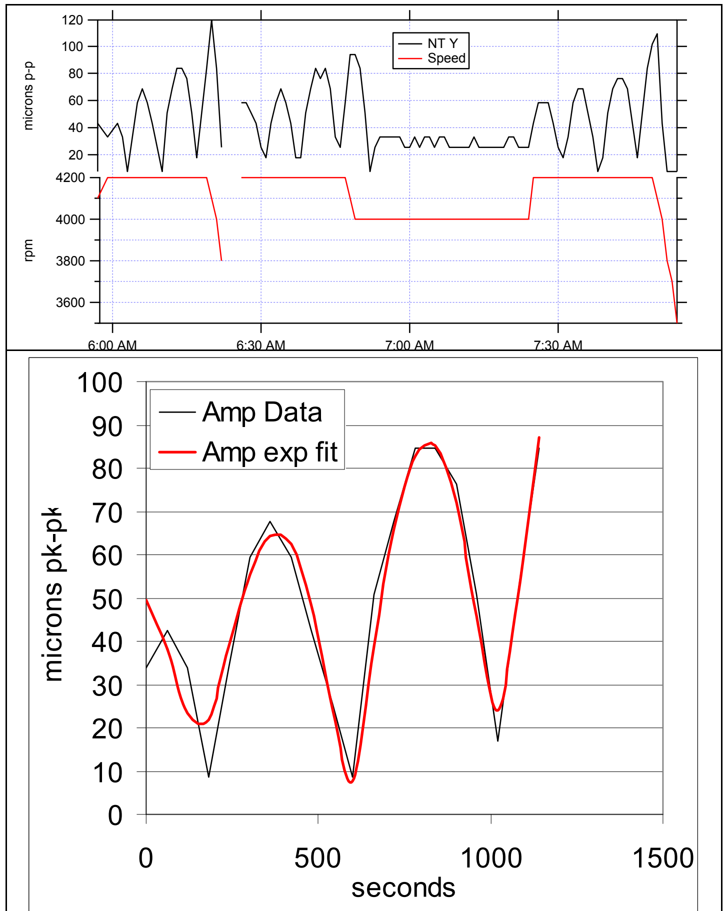

Period=456 sec, Growth rate=16%/minute

Figure 13. Event 3 – NTE Prox Probe Divergent Behavior.

approximately 12 to 38 minutes. The time constant of exponential vibration growth for unit 4 ranged from approximately 1.5 to 12 minutes. Units 1 and 2 exhibited stable Morton Effect vibration behavior at 4000 rpm (i.e. converging spirals upon reaching that speed). Unit 3 was oscillatory, but not divergent, at 4000 rpm. Example vibration data showing the oscillatory behavior at 4000 rpm is shown in Fig. 14. The divergent spiral of unit 3 at 4100 rpm is in Fig. 15, and from the curve fitting we can see a near textbook divergent spiral response. Unit 4 was rapidly divergent at 4000 rpm upon initial testing.

A significant observation from the test data for multiple machines is the relationship between vibration response levels prior to oscillatory behavior and/or divergence and how it may relate to Morton Effect stability. A tabular list of nominal synchronous housing velocity probe response levels for units 1, 2, 3, and 4 near the approximate 2500 rpm second critical speed and also upon first arrival at 4000 rpm is listed in Table 2. Unit 4 exhibited the most rapidly divergent behavior (largest amplitude growth and a reduced period of oscillation). Units 3 and 4 were markedly less stable at 4000 rpm compared to units 1 and 2, yet units 3 and 4 had significantly reduced response levels at 4000 rpm prior to the onset of oscillation and/or diverging spiral behavior. From the test data there appears to be a link between nominal synchronous response levels and stability of the Morton Effect. As the nominal synchronous response levels were reduced in subsequent machine builds, the stability of the machines was seemingly degraded when considering the reduced speeds at which divergent behavior was exhibited. As the machine residual imbalance appeared to improve from one unit to the next, the stability of the Morton Effect appeared to degrade.

The form of the single first order differential equation governing the behavior of the shaft temperature difference vector is given as Eq. (3) [3]. The solution for the temperature difference vector as a function of time takes the form of Eq. (4) [3]. The form of the eigenvalue for the solution of the single first order differential equation is provided in Eq. (5) [3]. The Morton Effect stability criterion provided in Eq. (2) is derived from the eigenvalue expression of Eq. (5). When the real component of the complex product of vectors $\vec{B}$, $\vec{A}$, and $\vec{C}$ approaches unity, the real component of the eigenvalue approaches zero. The equation for steady state synchronous vibration response in the absence of a thermal bow is shown in Eq. (6) [3]. With a stable thermal bow due to Morton Effect the equation for steady state vibration response is modified as shown in Eq. (7) [3]. The thermal sensitivity of the machine modifies the steady state vibration when the Morton Effect is present, even if it is stable. As discussed in [3], when the complex product of vectors $\vec{B}$, $\vec{A}$, and $\vec{C}$ is large, Eq. (7) indicates the Morton Effect will actually attenuate synchronous vibration. In other words, for machines which have a strong case of the Morton Effect, the mathematics of the Morton Effect presented in [3] suggest the vibration response may be reduced prior to the onset of instability. This serves as a possible explanation for the test data observation for units 3 and 4 where the synchronous response upon approaching 4000 rpm was markedly less than units 1 and 2, yet units 3 and 4 were notably less stable at 4000 rpm. The relationship between nominal synchronous response levels and instability severity suggests either better balance makes the Morton Effect worse or when the Morton Effect is worse the machine appears to be better balanced. There is no reason to suspect the former but we have reason to suspect the latter. Either way, the apparent relationship between nominal vibration response and Morton Effect stability exhibited by the machines in this case study cannot be ignored. Further study of explanations for this trend is of interest to the authors.

$$\tau\dot{\vec{T}} + \left(1 - \vec{B}\vec{A}\vec{C}\right)\vec{T} = \vec{B}\vec{A}\vec{U}_o \tag{3}$$

$$\vec{T}(t) = \vec{T}e^{st} \tag{4}$$

$$s = \frac{\vec{B}\vec{A}\vec{C} - 1}{\tau} \tag{5}$$

$$\vec{V}_{ss} = \vec{A}\vec{U}_o \tag{6}$$

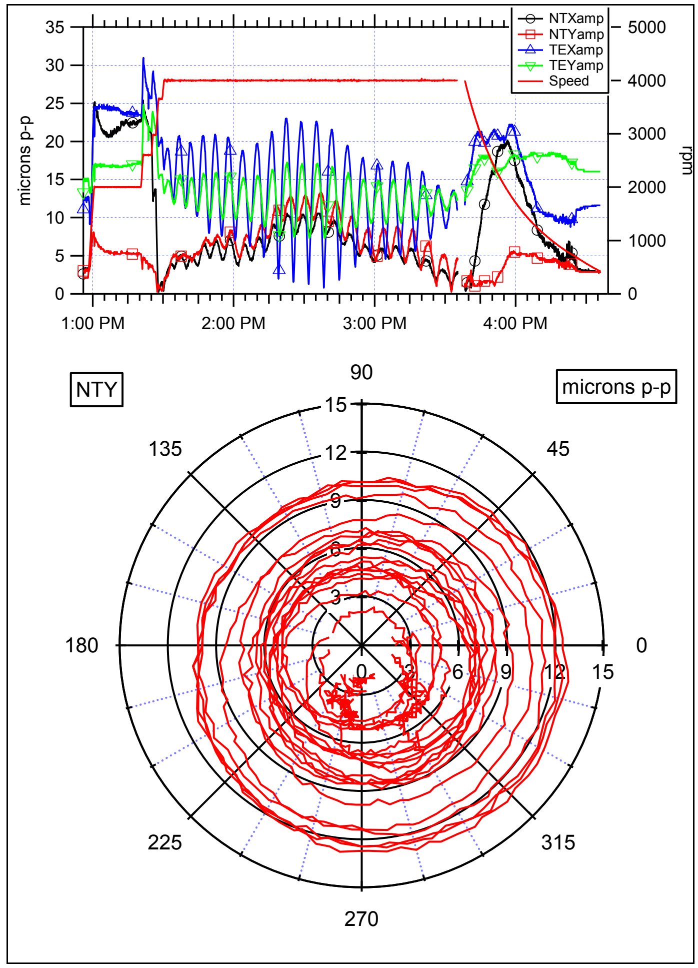

Figure 14. Unit 3 – Oscillatory Behavior at 4000 rpm.

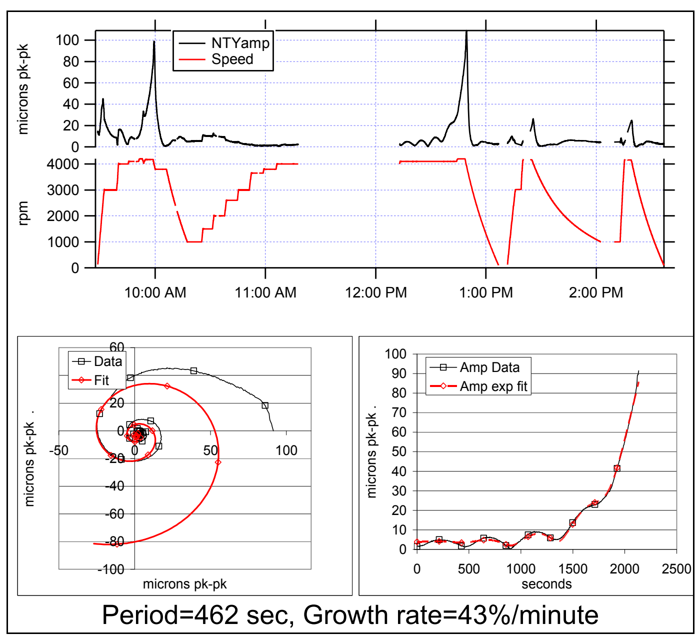

Figure 15. Unit 3 – Divergent Spiral at 4100 rpm.

$$\vec{V}_{ss} = \frac{\vec{A}}{1 - \vec{A}\vec{B}\vec{C}} \vec{U}_o \tag{7}$$

The mathematics presented in [3] suggest three possible states for the Morton Effect behavior depending on the magnitude of the real portion of the complex product of vectors $\vec{B}$, $\vec{A}$, and $\vec{C}$:

1. Re($\vec{B}\ \vec{A}\ \vec{C}$) < 1 → stable; converging spiral vibration
2. Re($\vec{B}\ \vec{A}\ \vec{C}$) = 1 → stability boundary; oscillatory yet not diverging spiral behavior
3. Re($\vec{B}\ \vec{A}\ \vec{C}$) > 1 → unstable; diverging spiral vibration

Figure 16 shows a sample of State 1 motion where Unit 1 executes stable spirals of increasing size at increasing speeds from 3000 to 4000 rpm. Each spiral is counterclockwise which implies the hot spot is traveling around the journal opposite the direction of rotation (plot uses lagging phase convention). These stable converging spiral response characteristics were found to be consistent for unit 1 at 4000 rpm. The machine repeatedly converged to the same basic nominal operating response point at 4000 rpm after following the converging spiral.

Unit 4 experienced the most rapidly divergent behavior upon first being tested in the factory (event number 9 in Table 1). Subsequent tests (events 10 and 11 from Table 1) yielded successive increases in the time constant of exponential growth; meaning it took longer for the machine to reach trip levels. Divergent spiral vibration data for unit 4 during event 10 is provided in Fig. 17. The physical changes to the machine hardware from one test to the next involved improvements to the residual imbalance of the overhung mass as well as improvements to the alignment of the spherically seated bearings. Even though the time constant of exponential growth was affected by the changes, the inherent instability of the machine configuration remained the same. The test data supports the hypothesis presented in [3] that Morton Effect stability (or lack thereof) is not a function of the time constant of exponential growth, and the dynamics of the hot spot motion need not be computed in order to asses the stability of the machine.

From the full suite of test data, each of the three states of stability for the Morton Effect were experienced in some manner among the four units with the original partial arc bearing. Examples of converging spirals, oscillatory behavior, and divergent spirals have all been presented.

The Morton Effect Analysis Results

The 13 step analysis process was applied to the original configuration with partial arc bearings. The process was repeated for various NTE bearing configurations in search of a potential hardware change solution. For the analyses of the potential bearing design changes, all other parameters in the

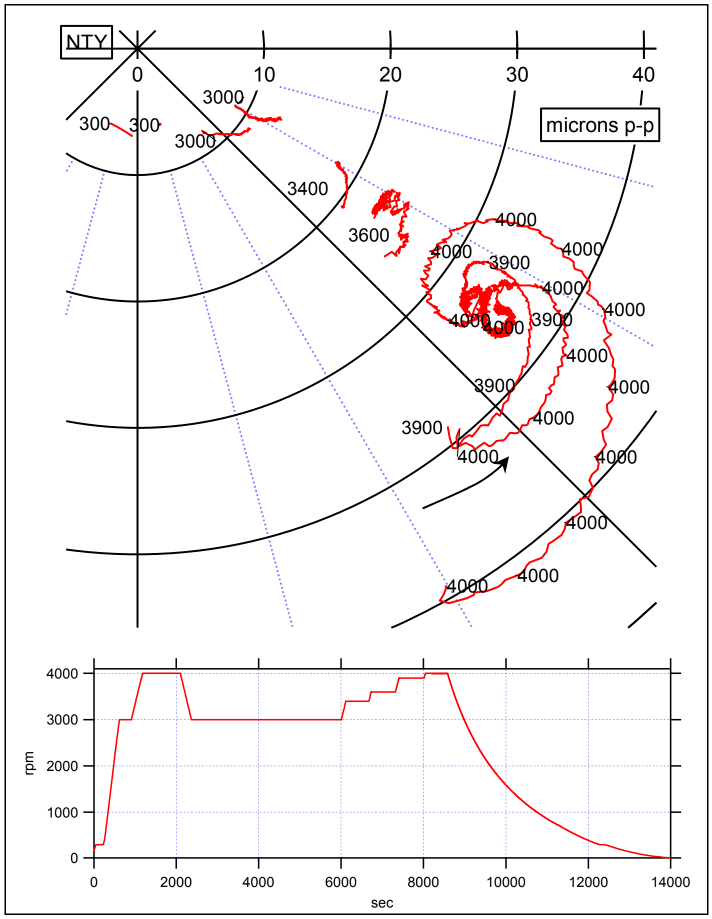

Figure 16. Unit 1 – Converging Spiral Vibration Behavior at speeds from 3000 to 4000 rpm. Labels on curves are rpm.

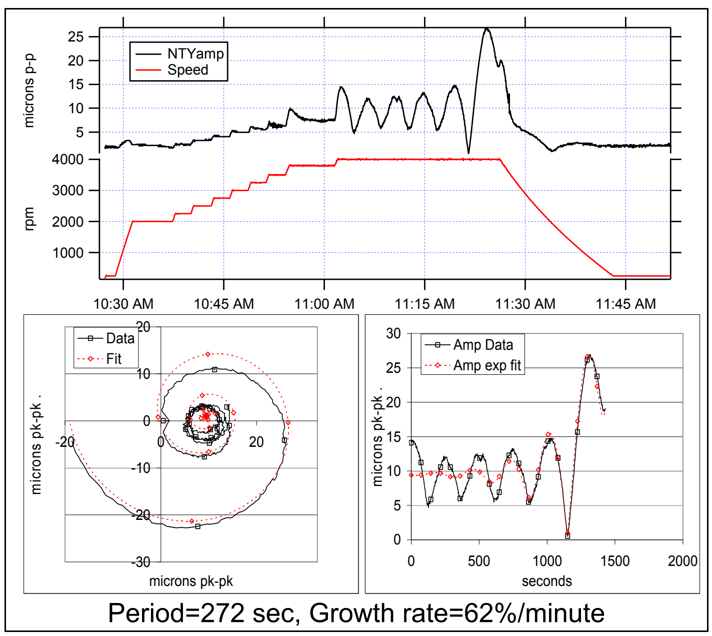

Figure 17. Unit 4 – Event 10 – More Rapidly Diverging Spiral Vibration Behavior at 4000 rpm.

modeling and simulation process were held constant while the details of the bearing geometry were changed. A host of different bearing types and geometries were considered (e.g. tilt-pad, fixed-pad, 3 lobe, 4 lobe, 5 lobe, preload, zero preload, etc.). Using the analysis method, a four lobe fixed pad bearing design (with zero preload) was identified as a potential solution (Fig. 3). Morton Effect stability plots in the complex plane and over a speed range of 3500 to 4500 rpm are presented in Fig. 18 for the original partial arc (PA) bearing design and the 4 lobe bearing (4L). The original PA bearing is predicted to exhibit unstable synchronous vibration behavior in the range of 3850 to 4200 rpm and this prediction agrees well with the test data. The figure shows that the instability with the PA bearing is predicted to desist at speeds above 4200 rpm. No testing was ever attempted above 4200 rpm, and the existence of an upper speed limit of the instability was not demonstrated. The calculations predict the 4L bearing configuration to be stable over the complete speed range. An important finding was that the calculation process exhibited a high degree of sensitivity to the fine details of the bearing thermal solution (and understandably so). Another key finding was that adjusting the thermal analysis options to produce the best match with measured bearing pad temperatures also produced the most accurate Morton Effect stability predictions. All calculations performed to date using best-known-good parameter values have demonstrated the potentially superior performance of the 4L bearing compared to the PA in this particular machine.

Calculated bearing oil film and shaft temperatures are shown in Fig. 19 for each bearing. Each of the 24 temperature curves in the two upper plots corresponds to a different orbit point solution from the bearing program. The temperature of any fixed point on the journal surface is obtained from each of these curves, but at a different circumferential location on each curve since the journal is turning, advancing 1/24th of a revolution from curve to curve. The dots in the upper plots represent the tracking of a single point (e.g. the high spot) on the journal from one curve to the next. From this data 24 temperatures are extracted for each journal surface point, and these are averaged to get the steady state temperature for that journal point. Doing this for many points around the journal leads to the bottom plot in the figure which shows calculated shaft circumferential temperature profiles for both bearings. Significant observations can be made from the data. The calculated maximum temperatures in the load zone are similar and this is consistent with test data where bearing RTD's are located near the high temperature load zone. However, the four lobe bearing has not only a smaller calculated shaft delta T value but also significantly lower average temperatures for any point on the journal believed due to the introduction of fresh lubricant at multiple locations.

Compete specifications of the bearings cannot be published due to proprietary concerns. The PA bearing has a 320 degree arc with its supply groove near horizontal (Fig. 3). The 4L bearing has a load on pad configuration with zero preload. For both bearings the nominal clearance ratio is 0.25%.

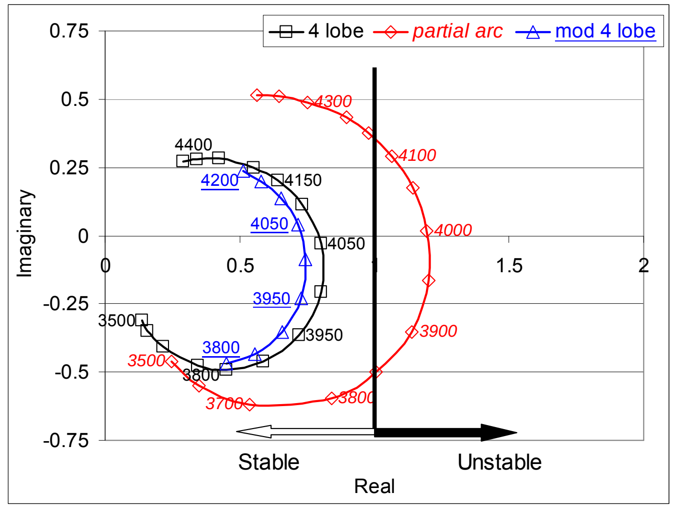

Figure 18. Morton Effect stability plotted in the complex plane – original partial arc bearing, 4 lobe bearing, and modified 4 lobe bearing. Labels on curves are rpm.

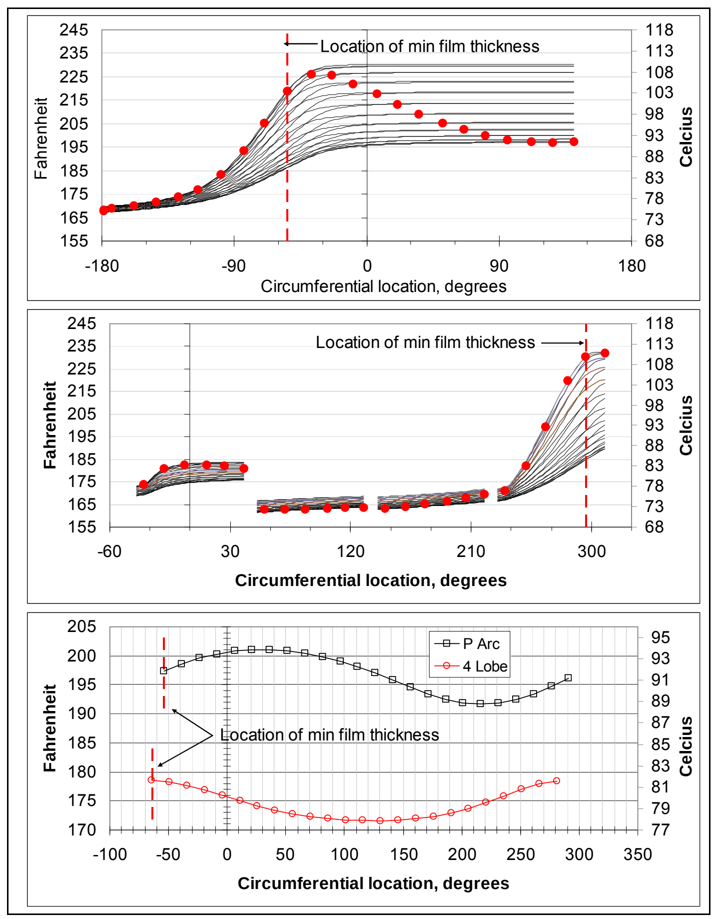

Figure 19. Oil Film and Shaft Temperature Results.

Change in Critical Speed

An undamped synchronous critical speed map is shown in Fig. 20 with the various bearing stiffness values plotted along with the frequencies of the first 3 rotor modes. The 4L bearing is seen to be less stiff than the PA in the horizontal axis, and stiffer in the vertical axis. The effect on the rotor critical speed nearest 4000 rpm (a mostly vertical mode per Fig. 6) is to increase it approximately 140 rpm per the undamped critical speed map. Forced response analyses (including damping) show a shift in the critical speed near 4000 rpm of approximately +100 rpm due to the bearing change. The damped forced response critical speed shifts from approximately 3925 rpm to 4025 rpm per the rotordynamic model calculations.

Based upon test data of the two configurations, the observed shift in critical speed due to the bearing change appears to be of a lesser magnitude than predicted, but this is subject to uncertainty due to the transient nature of the imbalance. A good estimate for the PA bearing critical speed comes from off-site testing where the observed critical speed is approximately 3975 rpm (Fig. 10). From a factory test shutdown from 4200 rpm of the first machine tested with the 4L bearing, the critical speed was observed to be approximately 4000 rpm. Test data thus indicated a shift of +25 rpm due to the bearing change. So, the shift in critical speed was both predicted and measured to move the critical closer to operating speed, and this works against the stabilizing capacity of the 4L bearing (see Fig. 18). However, the substantial thermal

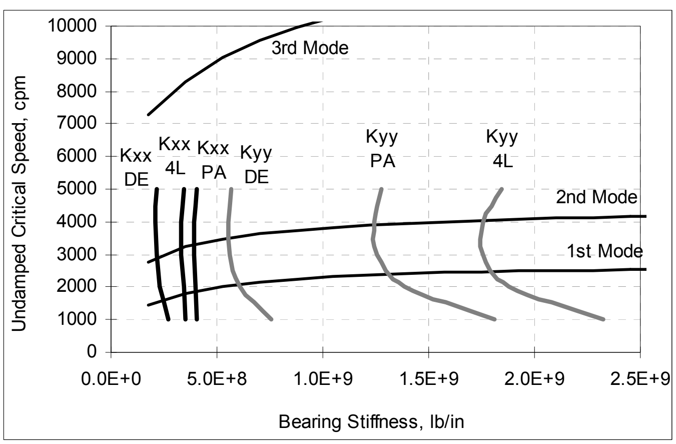

Figure 20. Synchronous undamped critical speed map as a function of bearing stiffness, with bearing stiffness data. DE=drive end PA bearing. PA & 4L are for NTE bearing.

improvement was still enough to eliminate the instability.

Four Lobe Bearing Test Results

As mentioned, a window of opportunity in the machine fabrication and qualification processes was opened due to the unstable behavior of unit 4 at 4000 rpm. A four lobe bearing liner was manufactured in short-order, and assembled into the unit 4 NTE bearing housing. At this point in time a specified test regiment had been put into place for assessing the synchronous vibration stability near maximum speed. The machine configuration with 4L NTE bearing was subjected to the stability test program and sample test results are in Fig. 21. The tests consisted mainly of holding at a constant speed for long durations and then incrementing the machine speed in relatively small increments and holding if stable operation was observed. The data in Fig. 21 is for the extended run at 4000 rpm for unit 4 with the new 4L bearing. This same test was previously attempted as part of the unit 4 testing with its PA bearing. There are small fluctuations in amplitude near the end of the test which are in-part related to manual adjustment of the bearing oil inlet temperature which in-turn affects the measured vibration response. As the bearing inlet oil gets warmer, the vibration response amplitudes increase and this is thought to be due to decreased oil film damping due to the thinner film. Examination of the proximity probe phase angles for the same test shows near constant behavior towards the ends of the test (Fig. 22). For comparison, results of the same series of tests on the same machine and test stand, but with the PA NTE bearing, are in Fig. 23. The data shows machine speed was held at 3800

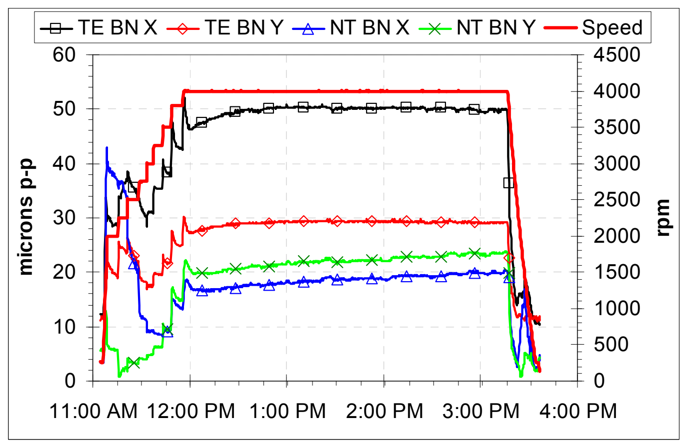

Figure 21. 4000 RPM Factory test of Unit 4, new 4 lobe bearing – prox probes 1x vibration amplitude vs. time.

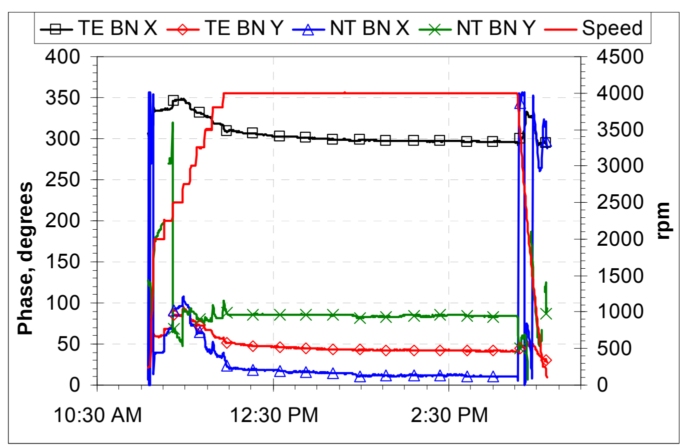

Figure 22. 4000 RPM Constant Speed Factory Test of Unit 4 with New 4 Lobe Bearing – Prox Probes 1x Phase

rpm for more than three hours and then incremented to 3900 and finally 3950 rpm. The unstable behavior shows itself toward the end of the 3800 rpm dwell, and then more so with each successive increase in speed. The machine was only able to run for approximately 30 minutes at 3950 rpm before having to be shut-down due to diverging spiral vibration. Once unstable divergent behavior was exhibited the machine was quickly shut-down to avoid potentially damaging levels of vibration. Conversely, for the new four lobe bearing, tests were successful up to and including a steady run for more than three hours at 4200 rpm (although the maximum normal operating speed of the machine was left capped at 4000 rpm due to sufficient energy density at 4000 rpm). A fifth unit was built and factory tested with the 4L NTE bearing, and test results for it are shown in Fig. 24. Units 1, 2, and 3 were subsequently field retro-fitted with the four lobe bearing. Vibration data has been fairly well monitored on the three retro-fitted field units and no instances of oscillatory and/or divergent vibration have been reported since the implementation of the four lobe NTE bearing. Additionally, units 4 and 5 also have not experienced any problems in the field.

Modified Four Lobe Bearing Analysis Results

After successful implementation of the four lobe bearing on the 5 units built, it was determined that the next phase of the program would require bearings capable of tolerating a significant amount of bearing load misalignment with respect to the vertical axis, due to potential global rolling motion of the machine. The four lobe bearing design used to successfully mitigate the Morton Effect problem was found to have insufficient tolerance to bearing load 'clocking' misalignment. Therefore, a new set of analyses were performed using the 13 step process to devise a potential solution for a bearing with adequate machine motion capability. Modifications to the angular location of the oil inlet ports for the existing four lobe bearing design were found to be a sufficient solution in that the modifications allowed for increased motion capability of the bearing as well as stable behavior was predicted by the Morton Effect analysis method. Figure 18 includes the Morton Effect stability results for the modified 4L bearing.

Modified Four Lobe Bearing Test Results

For the second phase of the program, three units have been built and factory tested with the modified four lobe bearing design and all units have exhibited stable vibration behavior during factory testing including the extended run factory test at 4000 rpm. Example time history traces of synchronous vibration amplitude during the extended run at 4000 rpm for phase 2-unit 2 are shown in Fig. 25. Similar results were obtained for the other two units built thus far in phase 2. The test results confirm the modified four lobe bearing to be another good solution in terms of mitigating the Morton Effect vibration instability experienced with the original PA NTE bearing design.

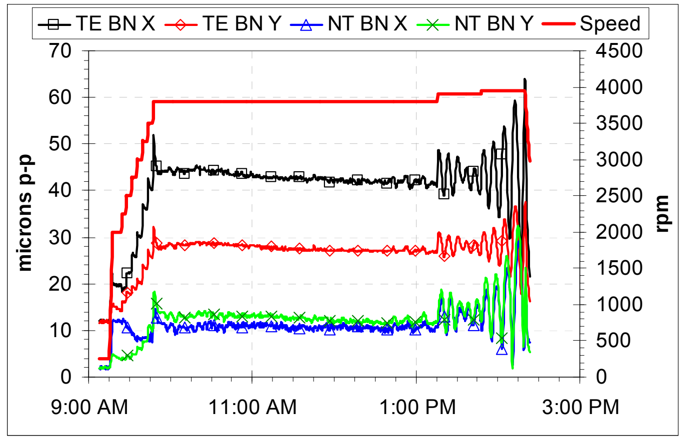

Figure 23. Factory test of Unit 4, original partial arc bearing (3800→3900→3950 rpm) – prox probes 1x vibration amplitude vs. time.

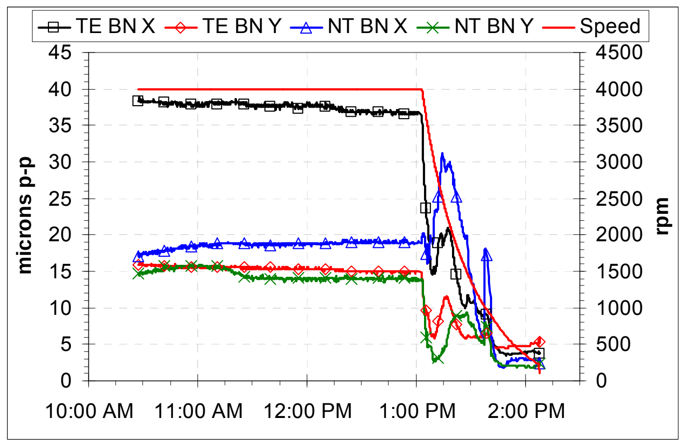

Figure 24. 4000 rpm Factory test of Unit 5, new 4 lobe bearing – prox probes 1x vibration amplitude vs. time.

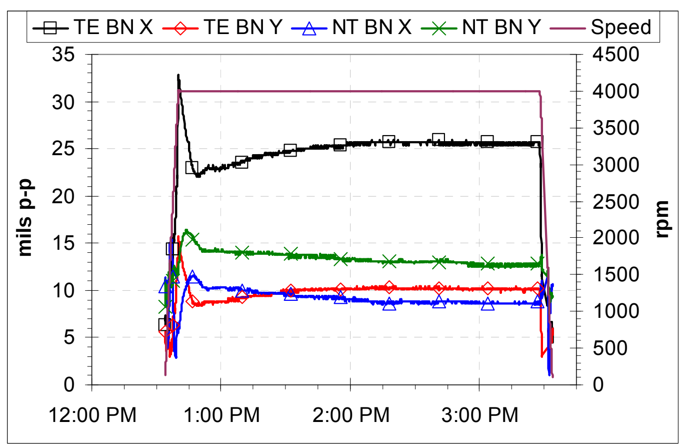

Figure 25. 4000 RPM Factory test of phase 2 Unit 2 with modified 4 lobe bearing – prox probes 1x vibration amplitude vs. time.

SUMMARY & CONCLUSIONS

Details of the method used to analyze machines for stability of the Morton Effect have been presented along with a case history for a machine which initially exhibited serious and potentially damaging synchronous vibration instability problems due to the Morton Effect.

The analysis method was used to evaluate potential solutions in the form of alternative bearing liner geometries. Based on the Morton Effect stability analysis, a 4 lobe bearing was subsequently built, implemented, and tested as a replacement for a partial arc bearing. The test results agreed with predictions as the modified bearing resulted in stable operation for all units tested. The ability to mitigate the instability problem with a bearing hardware change, and confirm the predicted behavior with test results, was viewed as a significant success by the end customer. To the authors' knowledge, this is the first published instance of a verified case of the Morton Effect to be solved exclusively by a change in bearing hardware with no accompanying changes to the rotor, shaft or journal.

This particular case study is unique in that all three potential scenarios for stability of the Morton Effect were experienced during testing on multiple machines of the same basic design. The three scenarios are 1) converging spiral vibration, 2) oscillatory vibration, and 3) diverging spiral vibration. The scenario experienced is dependent on the magnitude of the real component of the complex eigenvalue for the governing differential equation. Good agreement in terms of machine synchronous vibration behavior characteristics was found between the three stability behaviors hypothesized in [3] and the tests of the subject machines.

While the specific method of Morton Effect stability analysis shown here and presented in [3] is relatively new in the time frame of engineering sciences, based on the case history results presented here, the analysis method is viewed as a tool with significant potential for predicting the complex behavior of synchronous vibration instability due to the Morton Effect. The ability to quickly blend together rotordynamics, bearing thermal modeling, and simple mechanics calculations in a single post-processing routine results in a powerful tool which can be used to consider numerous design alternatives in a timely manner.

ACKNOWLEDGMENTS

The authors thank Kato Engineering and the Center for Electromechanics of the University of Texas at Austin for their support.

REFERENCES

[1] Keogh, P. S., and Morton, P. G., 1993, "Journal Bearing Differential Heating Evaluation with Influence on Rotor Dynamic Behaviour," Proceedings Roy. Soc. (London), Series A, Vol. 441, pp. 527-548.

[2] De Jongh, F. M., 2008, "The Synchronous Rotor Instability Phenomenon – Morton Effect," Proceedings of the 37th Turbomachinery Symposium, Turbomachinery Laboratory, Texas A&M University, College Station, Texas.

[3] Murphy, B.T., and Lorenz, J.A., 2010, "Simplified Morton Effect Analysis for Synchronous Spiral Instability," ASME Journal of Vibration and Acoustics, Vol. 132, October, 2010.

[4] Lorenz, J.A., 2009, "Implementation of Fluid-film Bearing Shaft Differential Heating Calculations Using Commercial CFD Software," University of Illinois at Urbana-Champaign, 2009.

[5] Dimarogonas, A. D. and Paipetis, S. A., 1983, *Analytical Rotordynamics*, Applied Science Publishers, New York.

[6] Murphy, B. T., 2010, "XLRotor 3.84 Documentation," Austin, Texas.

[7] Schmied, J. S., Pozivil, J., and Walch, J., 2008, "Hot Spots in Turboexpander Bearings: Case History, Stability Analysis, Measurements and Operational Experience." Proceedings of ASME Turbo Expo 2008: Power for Land, Sea and Air, Berlin, Germany, June 9-13, 2008. ASME Paper Number GT2008-51179.

